Book of Tutorials and Abstracts

European Microbeam Analysis Society

EMAS 2019

16th

EUROPEAN WORKSHOP

on

MODERN DEVELOPMENTS AND APPLICATIONS IN MICROBEAM ANALYSIS

19 to 23 May 2019
at the
NTNU, Realfagbygget
Trondheim, Norway

Organised in collaboration with:
Norwegian University of Science and Technology
(NTNU)

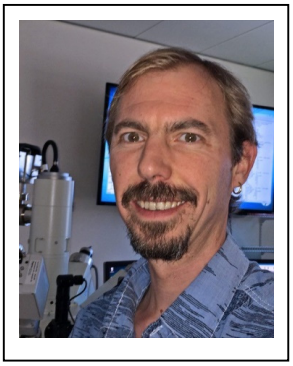

U-Th-Pb$_{TOTAL}$ DATING OF REE-PHOSPHATE BY ELECTRON MICROPROBE: REVIEW AND PROGRESS

Julien M. Allaz[1], M.J. Jercinovic[2] and M.L. Williams[2]

1 ETH Zürich, Inst. für Geochemie und Petrologie, Department of Earth Sciences
Clausiusstrasse 25, 8092 Zürich, Switzerland
2 University of Massachusetts Amherst, Department of Geosciences
611 North Pleasant Street, 233 Morrill Science Center, 01003-9297 Amherst, MA, U.S.A.
e-mail: julien.allaz@erdw.ethz.edu

Julien Allaz obtained an MSc, and a PhD in Geology at the Universities of Lausanne and Bern (Switzerland), respectively. During his early career, he focussed on structural geology and metamorphic petrology in the Swiss Alps, which required a large dose of electron microprobe analysis, some isotopic work (Ar-Ar dating and stable oxygen isotopes), and extended fieldwork. His attraction to the EPMA led him to the University of Massachusetts-Amherst from 2009, where he pursued a post-doc on trace element analysis and monazite dating by EPMA. In 2012, he became a Research Associate at the University of Colorado-Boulder and managed the electron microprobe laboratory. Since 2018, he is the head assistant for the electron microprobe and the scanning electron microscopy laboratories at the Institute of Geochemistry and Petrology at the Swiss Federal Institute of Technology in Zurich (ETH Zürich).

Julien's affection for the internet and for coding led him to the development of the "Database for electron Microprobe Analysis (De-MA)", which compiles essential information for EPMA users. In 2015, with the help of A. von der Handt and O.K. Neill, he initiated a Focussed Interest Group on MicroAnalytical Standards (FIGMAS: https://figmas.org) under the umbrella of both the Microanalysis Society and the Microscopy Society of America. This group aims to create an international database of standards and reference materials, and facilitate the development of tomorrow's reference materials. Julien has taken part in the organisation of the EPMA Topical Conference 2016 in Madison, WI, and at the forthcoming Quantitative Microanalysis Topical Conference 2019 in Minneapolis, MN. In 2016, he received the K.F.J. Heinrich award from the MAS society, which honours a young scientist for his distinguished technical contributions to the field of microanalysis. In 2017, he received the outstanding post-doc award from the University of Colorado Boulder. Author or co-author on 17 papers in internationally-recognised journals, Julien has also presented at over 25 conferences including 7 invited talks. His current research interests include magmatic and metamorphic petrology, geochronology, ore deposits (REE), and the development of new analytical setup for electron microprobe work and of databases for the EPMA community to help acquire precise and accurate data.

1. ABSTRACT

Monazite (Mnz) and xenotime (Xnt) are rare earth element (REE) phosphate minerals that occur in a large variety of rocks. They are known to contain very limited amounts of common Pb, and thus, a date can be calculated by simply measuring the total lead- and actinide-contents. Such a measurement can be done at high spatial resolution with an electron probe microanalyser (EPMA), together with a complete mineral analysis. The U-Th-Pb_{total} dating method was developed almost 30 years ago, to provide an in-situ age for several (U, Th)-bearing minerals such as uraninite, Mnz, and Xnt. This technique permits identification of events that are not recorded by other minerals, allows dates to be related to structural or geochemical features, and ultimately reinforces the age interpretation. The principal challenge is the accurate measurement of Pb, which is commonly present at the trace level (< 1,000 ppm).

This paper reviews the most recent advances in the U-Th-Pb_{total} dating technique of Mnz and Xnt, notably in terms of a) accurate background acquisition using the multipoint background technique, and b) improved peak interference correction for trace and REE elements. This paper also discusses a new method of quantitative element mapping, which helps with the identification of compositional domains in Mnz (or Xnt). Finally, a date cannot be interpreted as an age without the proper context, and several key factors in the interpretation are discussed and illustrated with several case studies.

2. INTRODUCTION

Geochronology is a part of the geological sciences that aims to determine the age of a rock, mineral, or domain within a mineral in order to constrain the age of some geological event. For instance, an age can be obtained from the decay of an actinide (^{238}U, ^{235}U, and ^{232}Th) to lead (^{206}Pb, ^{207}Pb, and ^{208}Pb) [1]. An isotopic analysis is commonly necessary in order to distinguish the daughter element of the decay from the initial amount of the element present in the mineral at its time of growth, e.g., the "common lead" in the U-Th-Pb decay series. However, several actinide-bearing minerals incorporate very little, if any, common lead, and a date can be obtained with a simple elemental analysis of U, Th and Pb. This is notably the case for uraninite, and for the REE-phosphates, monazite (Mnz) and xenotime (Xnt), for which the common Pb content is only a few ppm and essentially negligible compared to the Pb produced by the decay of the relatively abundant actinides [2, 3].

The U-Th-Pb_{total} dating technique was first applied on uraninite using an electron probe microanaysis (EPMA) [3, 4], followed in the nineties by its successful application to Mnz and Xnt [5-7] (see review in [8]). The vague term "chemical dating" is commonly used for this technique, and should be dismissed and replaced by "U-Th-Pb_{total} dating" or "electron microprobe dating" if an EPMA is being used, as any isotopic or elemental dating technique is "chemical" in essence. The U-Th-Pb_{total} dating technique of Mnz and Xnt can be subdivided into

two distinct approaches. First, the Chemical Isochron Method (CHIME) dating technique [7, 9-11] involves measurement of several Mnz (or Xnt, or zircon) of different compositions in order to obtain a "pseudo-isochron" of (Th,U) versus Pb, in which the slope is proportional to the date. All Mnz grains or domains included in the analysis should be within the error of the same age; otherwise results yield an age mixture or worse a totally spurious age. Whereas sector-zoned Mnz found in pegmatites and in some granitic rocks can satisfy this condition, it is rarely the case in metamorphic rocks, as the variation of Mnz composition indicates a different monazite-forming reaction and commonly, a different age. The second approach [5, 6] involves making a high-precision measurement of U, Th, and Pb from a chemically homogeneous domain established by X-ray mapping, (e.g., [12-19]). The goal is to link the date, or a population of dates from similar compositional domains, to specific mineral growth reactions. The single-domain age technique is applicable to any actinide-bearing phase providing the common Pb-content can be shown to be negligible. In this sense, the single-domain dating technique is more appropriate and will be the main focus of this paper.

The goal of this paper is to review the U-Th-Pb_{total} dating technique, and to discuss the recent improvements in the methodology, such as the peak interference corrections on REE and the utilization of the multipoint background approach for trace element analysis [14]. Novel approaches are also presented, notably a) quantitative element mapping to permit better targeting of a set of homogeneous domains for precise spot analysis, and b) the progress on a combined EDS-WDS analysis to reduce the overall acquisition time or to improve the precision on minor elements analysis, while preserving accuracy of the interpreted age.

3. MONAZITE AND XENOTIME

Mnz and Xnt are common accessory minerals that occur in a wide variety of geological settings, notably in (meta-)sedimentary rocks, placer deposits, gneisses, high-silica plutonic and volcanic rocks, and carbonatites [20]. They commonly display strong compositional zoning at the micrometre-scale, which can be related to magmatic, metamorphic, or hydrothermal reactions or events. Grains are commonly a few micrometres to 0.5 mm in size, and occasionally reach mm- to cm-size, notably in pegmatites. Mnz has a monoclinic structure and incorporates mostly light REE (La to Eu; LREE), whereas Xnt has a tetragonal structure with mostly Y and heavy REE (Gd to Lu; HREE). Actinides enter the mineral structure through the cheralite or the huttonite/thorite substitutions [21] (Table 1). Due to crystallographic constraints the solid solution towards cheralite or huttonite/thorite is incomplete, and Mnz incorporates up to 31.5 wt% ThO_2, with an average around 6 wt%, and a usually < 1 wt% UO_2 content [20, 22, 23]. The actinide content is generally higher in Mnz compared to Xnt. Monazite tends to prefer Th over U, whereas Xnt tends to prefer U over Th [24], although there are exceptions. Low temperature REE-phosphates tend to be poor in actinides and their compositions approach the ideal formulas of Mnz [LREE]PO_4 or Xnt [HREE]PO_4 [15], and the actinide content increases with temperature [25]. Other major substitutions in Mnz and Xnt are summarized in Table 1 [26-30].

Table 1. Possible substitutions in Mnz and Xnt. M^{2+} = divalent cation: Ca^{2+}, Sr^{2+}, etc.

Name	Substitution	End-member	Ref.	
Monazite-(Ce), Xenotime-(Y)	$LREE^{3+} \Leftrightarrow HREE^{3+}$	$REE(PO_4)$	-
Cheralite (brabantite)	$2\ REE^{3+} \Leftrightarrow Ca^{2+} + (U,Th)^{4+}$	$Ca(U,Th)(PO_4)_2$	[21]
Thorite, Huttonite, Coffinite	$P^{5+} + REE^{3+} \Leftrightarrow Si^{4+} + (U,Th)^{4+}$	$(U,Th)SiO_4$	[21]
Gasperite-(Ce), Chernovite-(Y)	$P^{5+} \Leftrightarrow As^{5+}$	$REE(AsO_4)$	[26, 27]
Sulfate (anhydrite, celestine)	$REE^{3+} + P^{5+} \Leftrightarrow M^{2+} + S^{6+}$	$M^{2+}(SO_4)$	[28-30]

Compositionally homogeneous domains are commonly in the range of a few microns, which necessitates the use of a high-spatial resolution analytical instrument. Mass spectrometry techniques, such as the laser-ablation inductively-coupled mass spectrometry (LA-ICP-MS), sensitive high-resolution ion microprobe (SHRIMP), or secondary ion mass spectrometry (SIMS) can provide excellent in situ isotopic analysis of U, Th and Pb. Yet, these techniques are spatially limited by their large ablation pit of 10 - 20 µm. Moreover, it is difficult to obtain a complete compositional analysis along with a date on these instruments, notably due to the lack of appropriate REE-rich standards in many laboratories for accurate measurement and the problem of isobaric interferences from $[REE]O^+$ compounds, which complicates the analysis of HREE (M. Guillong, pers. comm.). Access to these instruments, especially SIMS or SHRIMP, also remains limited, and their use can be expensive. EPMA U-Th-Pb_{total} dating offers an alternative with high spatial resolution down to the submicrometre scale [31]. However, limitations arise from the Pb detection limit, in general limiting its application to samples older than 100 - 200 Ma.

4. THE U-Th-Pbtotal AGE EQUATIONS

The very first approximate calculation of U-Th-Pbtotal age of Parslow *et al.* [4] using a single point analysis involved an iterative calculation of two equations to determine the Pb content that stems from the decay of U and Th:

$$t_U = 3.323 * 4.5 * 10^9 \left(\log\left[1 + \frac{x}{U}\right]\right) \quad (1a)$$

$$t_{Th} = 3.323 * 14 * 10^9 \left(\log\left[1 + \frac{Pb - x}{Th}\right]\right) \quad (1b)$$

where U, Th, Pb and x are atomic or molecular proportions, t_U and t_{Th} is the time in years, and the coefficients of each equation are related to the half-life of U and Th isotopes. The variable x is adjusted until the times t_U and t_{Th} converge. Shortly after, Bowles [3] proposed a single equation to iteratively calculate the date:

$$Pb = U * \left[0.9928\left(e^{\lambda^{238} * t} - 1\right) + 0.0072\left(e^{\lambda^{235} * t} - 1\right)\right] + Th * e^{\lambda^{232} * t} - 1 \quad (2)$$

where U, Pb and Th are atomic proportions, t is the time in years, λ^{238} (1.55125*10-10/y), λ^{235}(9.8485*10-10/y), and λ^{232} (4.9475*10-11/y) are the decay constants of ^{238}U, ^{235}U, and ^{232}Th [32], and the coefficients are the relative abundances of ^{238}U and ^{235}U. Equation 2 is very similar to the equation proposed by Montel et al. [5, 6], with the difference that U, Th and Pb are expressed as weight% or ppm:

$$Pb = 206\frac{U*0.9928}{238.04}\left(e^{\lambda^{238}*t}-1\right) + 207\frac{U*0.0072}{238.04}\left(e^{\lambda^{235}*t}-1\right) + 208\frac{Th}{232}\left(e^{\lambda^{232}*t}-1\right) \quad (3)$$

where 238.04 is the average atomic weight of U, and 232, 206, 207 and 208 are the atomic weights of ^{232}Th, ^{206}Pb, ^{207}Pb and ^{208}Pb. In Eqs. 2 and 3, the date is iteratively calculated to match the measured Pb-content (A Microsoft® Excel macro for the iterative calculation of Eq. 3 can be requested by email to JMA).

The approach of Suzuki and Adachi [7, 9, 33] is different and requires multiple analysis of Mnz domains of variable composition. The set of analyses is plotted in a PbO versus ThO_2* (or UO_2* for U-rich samples, e.g., Xnt or zircon) to obtain a "pseudo-isochron". ThO_2* is the total measured ThO_2 plus the equivalent UO_2:

$$ThO_2^* = ThO_2 + \left(\frac{UO_2*W_{ThO2}}{W_{UO2}*\left(e^{\lambda^{232}*t}-1\right)}\right)\left(\frac{e^{\lambda^{235}*t}+137.88*e^{\lambda^{238}*t}}{138.88}-1\right) \quad (4)$$

A first approximation of *t* in Eq. 4 is obtained by calculating an apparent date:

$$\frac{PbO}{W_{PbO}} = \frac{ThO_2}{W_{ThO2}}\left(e^{\lambda^{232}*t}-1\right) + \frac{UO_2}{W_{UO2}}\left(\frac{\left(e^{\lambda^{235}*t}+137.88*e^{\lambda^{238}*t}\right)}{138.88}-1\right) \quad (5)$$

where W_{PbO}, W_{ThO2}, and W_{UO2}, are the measured atomic weight of PbO, ThO_2 and UO_2. The date *T* is then obtained using the slope m of a regression on the PbO versus ThO_2* plot:

$$T = \frac{1}{\lambda^{232}}\ln(1 + m * \frac{W_{ThO2}}{W_{PbO}}) \quad (6)$$

The newly calculated time *T* is then inserted back in Eq. 4, and an iteration follows until *t* and *T* converge. The intercept of the regression of ThO_2* versus PbO is an indicator of the presence of common Pb. In the following, we will only consider the single-domain U-Th-Pb_{total} dating technique of Montel, yet the analytical considerations are applicable to all the above calculations.

The newly calculated time T is then inserted back in Equation 4, and an iteration follows until t and T converge. The intercept of the regression of ThO2* versus PbO is an indicator of the presence of common Pb. In the following, we will only consider the single-domain U-Th-Pbtotal dating technique of Montel, yet the analytical considerations are applicable to all the above calculations.

5. ANALYTICAL CONSIDERATIONS FOR EMP ANALYSIS OF Mnz AND Xnt

The use of EPMA to date Mnz and Xnt is advantageous due to a) the high spatial resolution reached by the EPMA (~1 μm^3 analytical volume at 15 keV; see extended discussion in [34]), b) the non-destructive nature of the analysis, c) the in situ character of the analysis, which preserves the textural and structural features, d) the capacity to collect element maps to identify the compositional variations, and e) the ability to simultaneously provide an U-Th-Pb_{total} age and a complete compositional analysis. The challenge lies in the precise and accurate measurement of U, Th and especially Pb, as the Pb-content is commonly < 1,000 ppm, which classifies this type of EPMA analysis as a trace element analysis [34, 35]. The numerous peak and background interferences from LREE, Y, Th and S, and the need for an accurate background correction complicate the analysis of Pb in REE-minerals, and the limitation of the technique arises chiefly from the detectability and analytical sensitivity of Pb, which restricts the application of the U-Th-Pb_{total} method to either old REE-phosphate (> 200 - 300 Ma) or to young and very actinide-rich chronometers (Fig. 1). Williams and Jercinovic [16] discussed the numerous pitfalls and ideal conditions for performing precise and accurate quantitative analysis, Jercinovic *et al.* [34] reviewed the optimal analytical conditions for trace element analysis, notably in Mnz, and this paper presents an updated analytical protocol (Table 2).

Table 2. Analytical protocols for Mnz or Xnt analysis by EPMA.

What	Comment	Analytical condition
1) Thin section preparation and coating (15-20 nm Al + 7-8 nm C or 20-30 nm C).	Aluminum coating preferred, thick (>20 nm) carbon coating possible, do not use Au or Ag coating (X-ray lines around Pb Mα, or U Mβ and Th Mα, respectively).	
2) Full thin section map with WDS or EDS phase map to identify accessory phases.	In samples with Ba-mineral, use La Lα to avoid interference of Ba Lβ on Ce Lα. Other element used as a base map, depending on the type of sample (e.g., Si, Al, or Mg Kα).	Stage mapping, 15 keV, 200-300 nA, defocused beam 20-30 µm, ca. 4-5 hours per thin section: Ce or La Lα (Mnz), Y Lα (Xnt), Ca or P Kα (apatite), Th Ma (Th-rich phase), other element.
3) Identification of accessory minerals (Mnz, Xnt, zircon, apatite), selection of 10-20 grains.	Selection of grain can be done based on structural considerations, shape of the grains, location of the grain with regards to other minerals, etc.	
4) Element mapping of individual Mnz and Xnt grains, ~10 to 20 grains.	For grains >50-100 µm, prefer either a mosaic image with several beam maps or a stage map to minimize defocussing effect. If Si- or Ca-content is very low, replace it by a REE.	Beam mapping, 15 keV, 200-300 nA, focused beam, <0.5 µm step size, ≥20-30 msec dwell time, usually 5-30 min per grain, Th Mα, U Mβ, Y Lα, Si Kα, Ca Kα (± REE).
5) (optional) Age map of monazite for illustrative purpose.	*Age mapping is a very long analysis, and only useful for high-Pb content and if a large age variation is expected.*	*Beam mapping, 15 keV, 200-300 nA, focused beam, <0.5 µm step size, ≥500 msec dwell time, usually 8-12 hours per grain, Th Mα, U Mβ, Pb Mα, Y Lα.*
6) Complete quantitative analysis (U, Th, Pb, P, REE, etc; see Table 4).	Alternative option: two-step combined analysis with (a) low current (20 nA) analysis of major element, and (b) high current (200 nA) analysis for minor and trace elements.	15 keV, 200 nA, focused beam, 10-15 min per point (peak only), 5 to 8 points per homogeneous domain, combined with EDS analysis for P (±REE). See details in Table 3.
7) Data treatment and age calculation	Age calculation following Montel's method [5,6], one age per homogeneous domain (average of 5-8 points), bring together full thin section, grains maps, and age data.	

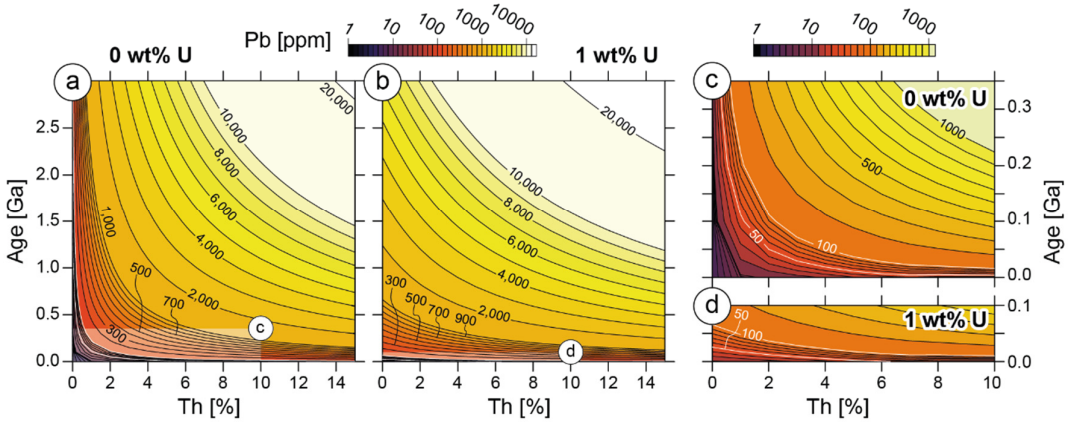

Figure 1. Production of Pb as a function of the age and Th-content assuming a) 0, or b) 1 wt% U. c, d) Enlargement of a, b). Limitations of the technique arise at Pb content < 50 - 100 ppm (white lines).

5.1. Instrumentation and analytical conditions

Most data considered here were obtained on a 5-spectrometer JEOL JXA-8230 EMP at the University of Colorado-Boulder equipped with a W filament (~1.2 µm focused beam diameter at 15 keV, 200 nA) or a LaB_6 cathode (~0.7 µm). Some data were obtained on a CAMECA SX-100 "Ultrachron" EPMA at the University of Massachusetts-Amherst equipped with a LaB_6 or CeB6 cathode. Both instruments have a 10 mm2 EDS detector, yet only the JEOL instrument was used for combined EDS-WDS analysis. Complementary tests were also obtained at ETH Zürich using a JEOL JXA-8200 and a scanning electron microscope JEOL JSM-6390 equipped with a 30 mm^2 Thermo UltraDry SDD EDS detector. A summary of the detector and spectrometer configurations is listed in Table 3. Unless specified otherwise, analytical conditions were 15 keV, 200 nA and a focussed beam (see also Table 2).

Table 2. EPMA configurations used in this study.

	Cameca SX-100		JEOL JXA-8230		JEOL JXA-8200	
1	TAP	P-10, low P	TAP	P-10, low P	PET	P-10, low P
2	L-PET	P-10, high P	L-PET	P-10, low P	H-TAP	P-10, low P
3	VL-PET	P-10, high P	L-PET	Xe sealed	LiF	Xe sealed
4	VL-PET	P-10, high P	L-PET	Xe sealed	H-PET	Xe sealed
5	L-LiF	P-10, high P	L-LiF	Xe sealed	H-PET	Xe sealed
EDS	Bruker XFlash 4010		Thermo UltraDry		JEOL SiLi EDS	

5.2. Monazite identification and element mapping

A highly polished thin section is necessary for accurate analysis. After cleaning, the thin section is coated with either a thick C-coating or an Al-coating with a thin overcoat of C to prevent the rapid oxidation of Al. A dual (Al+C)-coating is preferred, as it significantly minimizes the beam damage effect compared to C alone [36].

The first step is to identify all Mnz and Xnt grains in the thin section in order to select a representative set of grains. Identification of accessory phases in the thin section can be done either with a phase analysis map using the energy-dispersive spectrometer (EDS) or with a full thin-section element map using the wavelength-dispersive spectrometers (WDS) and scanning for Ce-Lα or La-Lα (Mnz), Y-Lα (Xnt), Ca or P-Kα (apatite), Zr-Lα (zircon), and a major element map (e.g., Si-Kα, Al-Kα, or Mg-Kα) or a BSE image to be used as a base map (step 2 in Table 2; e.g., [37]). Even with a step size of 20 - 30 μm (and equivalently defocussed beam), Mnz or Xnt grains as small as 5 μm can be identified with the full thin section WDS maps as these phases are usually the only ones to incorporate a large quantity of Ce or Y, whereas an EDS phase analysis map usually requires a smaller pixel size to permit the proper identification of 5 - 10 m-sized phases. A faster identification by EDS can be performed with a dedicated particle search software that uses a threshold on a mosaic BSE image to highlight dense particles, completed by an EDS identification of each particle, with the caveat that the thresholding must be set to reveal the smallest target grains in the section.

In the second step, a number (10 to 15 minimum) of individual Mnz or Xnt grains per sample are mapped using the WDS to reveal the variation of Th-Mα, U-Mβ, Y-Lα, Ca-Kα and Si-Kα (step 3 in Table 2). EDS mapping is not useful here, as it does not have the required sensitivity to reveal all the compositional variations. Moreover, there is a critical interference between P-Kα and Y-Lα, which will obscure small Y variations. In order to permit an inter-grains and even an inter-samples comparison, the maximum and minimum intensity levels of each map should be treated simultaneously [38], or the maps should be quantified (see example below). The grains are targeted in order to have a representative set of all sizes, shapes, and textural or structural context in order to capture all possible compositional and textural variations in the Mnz and Xnt populations.

High-resolution element mapping of Th-Mα, U-Mβ, Y-Lα, and Pb-Mα at very high current (> 500 nA) and long counting time (0.5 - 1 s per pixel; step 4 in Table 2) can provide low precision age maps for Mnz grains [39]. At these conditions, a single map of a 50 - 100 μm grain can easily take 8 - 12 hours to complete, whereas in the same amount of time multiple grains can be quantitatively analysed and dated with higher precision. High-resolution age mapping is, therefore, recommended mainly for an illustrative purpose, where complexly zoned grains present a strong contrast in age domains. A single-domain quantitative analysis should remain the rule to provide precise data.

5.3. Quantitative analysis

The U-Th-Pb_{total} analysis of Mnz or Xnt by EMP must be considered as a "trace element analysis" [34, 35], as Pb, some REE, and sometimes U or Th are commonly found in trace amounts (< 1,000 ppm). The use of a high beam current, long count times, and a set of high count-rate spectrometers is thus, necessary. This type of analysis is challenging due to a) the non-linearity of the background, b) the presence of numerous peak and background interfering

X-ray lines, notably from Th and REEs, and c) a high potential for beam damage during the analysis. The following is a summary of some of the key analytical considerations necessary to obtain an accurate U-Th-Pb_{total} date and a complete compositional analysis (step 4 in Table 2). A generalised analytical setting suitable for both Mnz and Xnt analysis is summarized in Table 4. One or more secondary Mnz (or Xnt) reference materials of known age are measured before, during, and after the analysis of unknowns in order to ensure that the analytical protocol and that the results are consistent from day to day (= "age consistency standard"). Recently Goncalves *et al.* [40] has reviewed several Mnz reference materials from Brazil that are suitable for isotopic or elemental analysis. In this study, the Moacyr Mnz (TIMS age ~507 Ma; equivalent to the Itambé Mnz [40]) and Burnet Mnz (SIMS age ~1088 Ma) are used as reference materials.

Table 4. Analytical setting for Mnz and Xnt analysis by EPMA.

SP	El.	Line	Xtal	Peak [mm]	Peak [10^5.sinθ]	Recommanded standard	Time [s] Peak	Time [s] Bkg#	Bkg Type	Major and minor peak interferences (see Table 7)	
1	Y	Lα	TAP	69.70	24890	YPO_4	180	-	MAN	Sr Lβ	(1)
1	*Sr*,***	*Lα*	*TAP*	*74.77*	*26705*	*Strontianite*	*180*	-	*MAN*	*Si Kβ + satellite peaks*	
1	Si	Kα	TAP	77.10	27535	Microcline	180	-	MAN	Nd Lα (III)	
1	*As*,***	*Kα*	*TAP*	*105.36*	*37630*	*As-pyrite, GaAs*	*180*	-	*MAN*	*Tb Mβ; Dy Mα; Sm Mγ*	
2	Th	Mα	L-PET	132.44	47300	$CaTh(PO_4)_2$, ThO_2	550	50##	MPB	-	
2	Ca	Kα	L-PET	107.50	38395	Apatite	60	-	MAN	-	
2	S	Kα	L-PET	172.09	61460	Sulfate or sulide	60		MAN	-	
3	U	Mβ	L-PET	119.04	42470	UO_2	600	50##	MPB	K Kα; Th Mγ; Sm $Lβ_2$ (II)	
3	K	Kβ	L-PET	110.64	39515	K-feldspar	100	-	MAN	U Mγ; Tm Lα (II); Ca Kα	
4	Pb	Mα	L-PET	169.24	60445	Pyromorphite	700	50##	MPB	Y $Lγ_{2,3}$; Th Mζ; La Lα (II)	(2)
5	*La***	*Lα*	*L-LiF*	*185.38*	*66205*	*$LaPO_4$*	*30*	-	*MAN*	*Nd Ll*	*(3)*
5	Ce	Lα	L-LiF	178.12	63615	$CePO_4$	30	-	MAN	-	(3)
5	Nd	Lα	L-LiF	164.82	58864	$NdPO_4$	30	-	MAN	Ce Lβ; La $Lβ_6$	(3)
5	*Pr***	*Lβ*	*L-LiF*	*157.08*	*56100*	*$PrPO_4$*	*30*	-	*MAN*	-	*(3)*
5	Sm	Lβ	L-LiF	138.97	49630	$SmPO_4$	30	-	MAN	Tb Lα	(3)
5	*Tb**	*Lα*	*L-LiF*	*137.41*	*49075*	*$TbPO_4$*	*60*	-	*MAN*	*Sm Lβ*	
5	Eu	Lβ	L-LiF	133.58	47705	$EuPO_4$	60	-	MAN	Dy Lα	(4)
5	Dy	Lα	L-LiF	132.66	47380	$DyPO_4$	60	-	MAN	-	
5	*Er**	*Lα*	*L-LiF*	*123.98*	*44280*	*$ErPO_4$*	*60*	-	*MAN*	*Tb Lβ*	
5	Gd	Lβ	L-LiF	128.32	45830	$GdPO_4$	60	-	MAN	Ho Lα; $Lβ_2$	(4)
5	*Tm**	*Lα*	*L-LiF*	*119.96*	*42845*	*$TmPO_4$*	*60*	-	*MAN*	*Sm Lγ; Dy Lβ; Gd $Lβ_{9,10}$*	(5)
5	Yb	Lα	L-LiF	116.13	41475	$YbPO_4$	60	-	MAN	Tb $Lβ_{2,15}$; Dy $Lβ_{3,6}$; Sm $Lγ_2$	
5	*Ho**	*Lβ*	*L-LiF*	*114.40*	*40855*	*$HoPO_4$*	*60*	-	*MAN*	*Yb Lα,n; Dy $Lβ_{2,15}$*	
5	*Lu**	*Lα*	*L-LiF*	*112.62*	*40220*	*$LuPO_4$*	*60*	-	*MAN*	*Ho $Lβ_{3,6}$; Dy $Lβ_{2,15}$; Eu Lγ*	
-	P	Kα	EDS	2.01 keV		$CePO_4$	300	-	EDS	Y Lβ	(6)

*, **: minor to trace element in Mnz (*) or in Xnt (**).
Background measurement is done separately from the peak measurement (see text for discussion).
The MPB background counting time can be increased to 100 s for higher precision.
MAN: Mean Atomic Number background correction; MPB: Multipoint Background correction.
(1) Consider analysing Y-Lα on a PET (SP 2) if the line is too close to the spectrometer limit.
(2) Use Pb-Mβ for Xnt. If U-Mβ is analysed on the same spectrometer as Th-Mα, two spectrometers can be used for Pb analysis to enhance precision.
(3) To gain time, the main LREE elements can be analysed by EDS, at the cost of a lower precision.
(4) Strong interferences on Eu-Lβ and Gd-Lβ in Xnt; prefer Eu-Lα and Gd-Lα.
(5) Strong interference of Sm-Lγ on Tm-Lα in Mnz; Tm- Lβ could be an alternative option, although it is strongly interfered by Gd-$Lγ_2$ and Tb-Lγ (not tested here).
(6) P-Kα is best analysed in Mnz by EDS in order to minimize beam damage effect. Alternatively, P-Kα can be analysed by WDS with a PET monochromator (required for Xnt due to interference from Y-Lα).

5.3.1. Choice of spectrometer. It is necessary to select a spectrometer that yields a high count-rate with a high peak-to-background ratio, in order to lower the detection limit and increase the analytical sensitivity for the analysis of minor and trace elements. Integrating counts from one or more spectrometers measuring the same element, a common feature of modern software, can increase precision substantially. A comparison of the count rate obtained on UO_2, ThO_2, pyromorphite, and a few REE phosphate standards on JEOL or CAMECA instruments (Table 5) demonstrates the large gain in intensity using a spectrometer equipped with large- (L-type crystals) or very large area monochromators (VL-type PET monochromator on Cameca only), or a spectrometer with a smaller Rowland circle (H-type; on JEOL only) compared to a normal spectrometer (J-type). For the selected elements, a count-rate gain of 2.1 to 3.2x is observed between J-type and L-type spectrometers equipped with Xe counter, and of 2.7 to 4.1x between J-type and H-type spectrometers (Table 5). A disadvantage of the H-type spectrometer is the loss of spectral resolution compared to J- or L-type spectrometers (Fig. 2a), which complicates the selection of an appropriate background and increases the effect of peak interferences, especially for REE analysis. The H-type spectrometer also has a higher background and a lower peak-to-background ratio compared to the VL- or L-type spectrometers (Table 5; Fig. 2b). This reduces its sensitivity despite the higher count rate. In terms of count rate, the L-type spectrometer appears to be superior compared to the H-type spectrometer for X-ray lines of energy > 6.4 keV (Table 5). In the present study, tests of VL-type spectrometer from CAMECA are only shown for the measurement of Pb-Mα, for which this spectrometer was designed, and U-Mβ. This spectrometer beats all others with a high-count rate, a good peak-to-background ratio, and a similar spectral resolution compared to the L-type spectrometers. The use of a Xe-counter or a high-pressure (2 - 3 atm) Ar-counter is recommended for the analysis of medium to high energy X-ray lines, with a small advantage to the high-pressure Ar-counter on intermediate X-ray lines energies (4.0 - 6.4 keV) and to the Xe-counter on lower or higher energies, although the difference is only ±20 - 30 % relative, and is likely to be dependent on the spectrometer alignment.

An optimum instrument for trace element analysis should be equipped with an L-type spectrometer for REE, U, and Th analysis, and with an L- or even better, an H- or VL-type spectrometer for the analysis of Pb-Mα, with either a high-pressure Ar-counter or a Xe-counter. Figure 3 shows the detection limits obtained on L-type spectrometers for the analysis of U, Th, Pb and REE (see [14, 34] for a detailed discussion on detection limits and sensitivity). In the case of Mnz or Xnt analysis, it is desirable to reach at least a 30 to 50 ppm detection limit on Pb-Mα, which is achievable after 5 to 10 min counting time at 200 nA on a L-, VL-, or H-type spectrometer. The detection limit of ppm on Lα- or Lβ- lines after 30 s counting on the peak at 200 nA, and 90 to 180 ppm after 60 s counting (Fig. 3).

A danger of using a high count-rate spectrometer is an inaccurate dead time correction and a potential shift of the pulse in the X-ray detector, the latter being significant on JEOL instruments due to the smaller detector size and the absence of an exit window. The deadtime correction

Table 5. Comparison of count-rate and peak-to-background ratio for J-, L-, H- or VL-type spectrometers.

				Net peak [cps/nA]						Peak-to-background ratio					
				J-type	J-type	L-type	L-type	H-type	VL-type	J-type	J-type	L-type	L-type	H-type	VL-type
	Standard	X-ray	keV	Ar, LP	Xe	Xe	Ar, HP	Xe	Ar, HP	Ar, LP	Xe	Xe	Ar, HP	Xe	Ar, HP
PET	Pyromorph.	Pb Mα	2.35	61.1	66.5	141.2	145.1	239.3	266.4	27.0	124.9	195.7	242.9	116.1	179.8
PET	ThO_2	Th Mα	3.00	72.5	151.6	397.1	-	563.1	-	15.9	82.1	153.7	-	78.3	-
PET	UO_2	U Mβ	3.34	69.3	166.4	336.5	280.4	636.0	420.2	11.4	80.2	83.1	63.0	74.5	56.7
LiF	$LaPO_4$	La Lα	4.65	-	22.2	62.2	88.7	91.8	-	-	101.1	137.8	106.6	78.3	-
LiF	$NdPO_4$	Nd Lα	5.23	-	37.1	98.9	121.0	137.0	-	-	104.2	125.7	100.2	75.7	-
LiF	$TbPO_4$	Tb Lα	6.27	-	54.3	144.7	164.3	172.6	-	-	70.3	82.2	63.0	48.4	-
LiF	$DyPO_4$	Dy Lα	6.49	-	57.0	184.1	168.1	177.2	-	-	61.4	73.2	61.5	42.2	-
LiF	$HoPO_4$	Ho Lβ	7.52	-	36.1	114.0	89.5	98.8	-	-	26.8	25.7	21.5	16.7	-

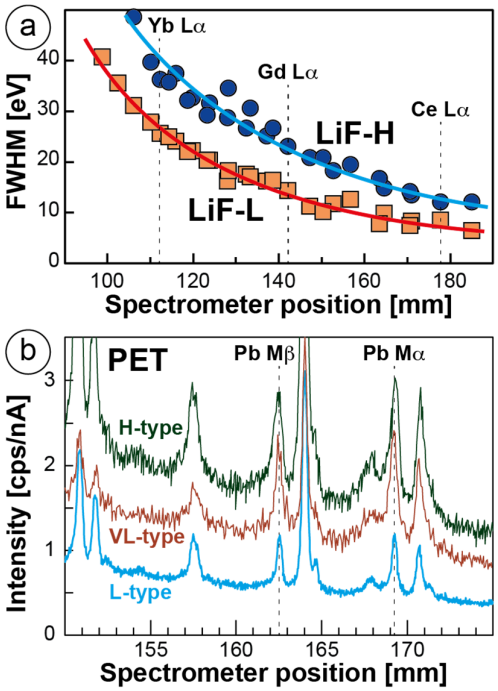

Figure 2. a) Variation of the full-width at half maximum (FWHM) on Lα and Lβ X-ray lines of REE on L-type versus H-type spectrometer (LiF). b) Comparison of scans around Pb-Mα obtained on L-, VL-, and H-type spectrometers (PET) in Burnet Mnz. WDS scan on L-type spectrometer acquired with higher precision.

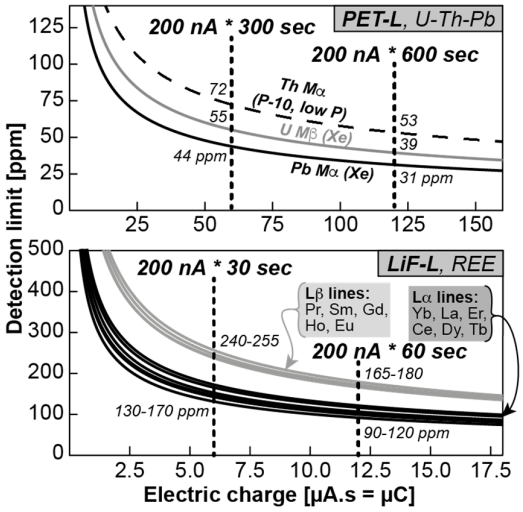

Figure 1. Detection limits on L-type spectrometers for U, Th, Pb (PET-L) and REE (LiF-L)..

should be carefully checked regardless of the detector, especially for the major elements (e.g., La, Ce, Nd, Th) that are analysed at high current with a standardisation done at low current and when the count rates are above ~20 - 30k. It is recommended to keep the PHA setting of those elements either in integral mode or in differential mode with a significantly large window to accommodate a possible pulse shift. Conversely, an optimum PHA window setting for X-ray lines interfered by high-order X-ray lines should be set to minimise this type of interferences (e.g., La-Lα□ [n=2] on Pb-Mα)

5.3.2. Background acquisition. An accurate background measurement is absolutely essential for trace element analysis [34]. In fact, one could go so far as to say that trace element EPMA analysis is mostly an exercise in characterising background at high precision and accuracy. Gathering peak counts at high precision is obviously a consideration, but if the background is inaccurate, the result may be meaningless (as P/B nears unity). It is well established that the X-ray continuum is not perfectly linear and is better modelled using an exponential or a polynomial curve [14, 16, 34]. Moreover, the background positions must be chosen in order to avoid any background interference. Numerous interfering X-ray lines are present around Pb-Mα and -Mβ, notably Y-Lγ$_{2,3}$, Th-Mζ, and several 2nd order lines of LREE (La, Ce, Pr; Fig. 4a). Further complications can arise from additional X-rays from unexpected elements that are either rarely present (e.g., S-Kα,β in Moacyr; Fig. 4a) or induced by secondary fluorescence at distance from a neighbouring phase (e.g., Ti- Kα or K-Kα; [41]).

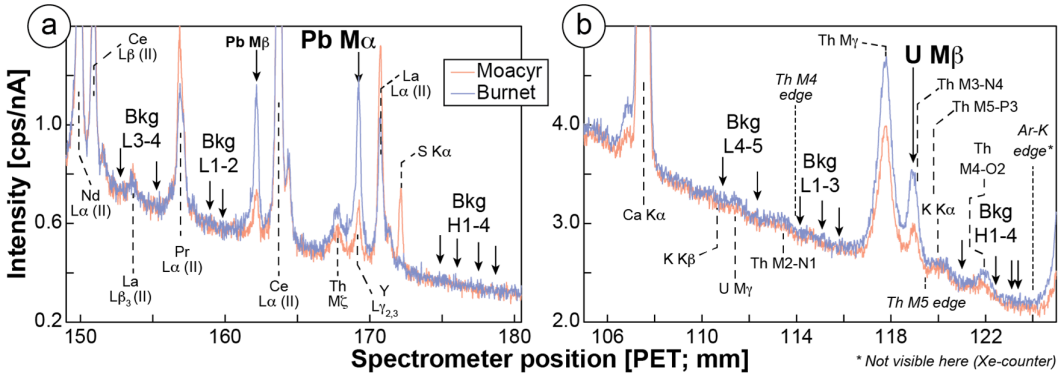

Figure 4. WDS scans acquired on L-type monochromator (PET-L) in Moacyr and Burnet Mnz around a) Pb-Mα, and b) U-Mβ with multipoint background positions on low (Bkg Lx) and high side (Bkg Hx).

Williams and Jercinovic [16, 42] initially suggested acquiring a detailed quantitative (step, not time-sliced ROM, scan yielding accurate, dead-time corrected cps/nA) WDS scan at high current (≥ 200 nA) around the X-ray lines of U-Mβ, Th-Mα and Pb-Mα, and to use this scan to accurately determine the background intensity by taking into account the background curvature and avoiding the background interferences. Because the background value is directly dependent on

the composition (i.e., the average Z), a single WDS scan is necessary within each homogeneous domain. While this technique remains accurate, it is time-consuming and subjective, as the analyst has to select areas in the scan, which appear to represent the background. Moreover, minor background interferences might be barely visible and lost in the low analytical precision of a WDS scan unless a very long counting time is used.

A better background measurement technique called the "multipoint background acquisition" has recently been developed [14]. This method involves measurement of several background intensities (perhaps 6 or more) at pre-set spectrometer positions around the peak of interest, and the acquired intensities are interpolated with a linear or better an exponential or polynomial fitting in order to accurately and precisely determine the background curvature and intensity. The set of background positions is selected based on a collection of WDS scans in a series of materials similar to the unknowns being analysed (Table 6; Figs. 4a and 4b). This approach is less subjective than the WDS scan technique, and it tolerates a few erroneous background positions that are affected by one or more unexpected background interferences in a specific sample. Erroneous background(s) are removed during the reprocessing either automatically by selecting the points that yield the statistically lowest background (within the precision of the acquisition) or manually by the analyst. The technique has been successfully tested in multiple Mnz reference materials for which an isotopic age exists (see details in [14]).

Table 6. Multipoint background positions for the analysis of U-Mβ, Th-Mα, Pb-Mα and Pb-Mβ.

		Cameca position [10^5 sinθ]				JEOL position [mm]			
		U Mβ	Th Mα	Pb Mα	Pb Mβ	U Mβ	Th Mα	Pb Mα	Pb Mβ
Bkg Low	1	-1095	-1035	-3200	-375	-3.0	-2.9	-9.0	-1.0
	2	-1355	-1270	-3500	-2800	-3.8	-3.5	-9.8	-7.8
	3	-1685	-1470	-4750	-3760	-4.7	-4.1	-13.3	-10.5
	4	-2330	-	-5460	-4000	-6.5	-	-15.3	-11.2
	5	-2850	-	-	-	-8.0	-	-	-
Bkg High	1	760	1940	1900	430	2.1	5.4	5.3	1.2
	2	1265	2600	2300	935	3.5	7.3	6.4	2.6
	3	1525	3780	2800	1100	4.2	10.6	7.8	3.1
	4	1600	-	3200	1750	4.5	-	9.0	4.9

Background acquisition for the REE is also challenging, as multiple X-ray lines prevent the selection of a "true" background position, especially for the HREE. The "shared background" method [14] can be used to minimise the risk of a background interference and to correct for the effects of absorption edges. In this paper, we consider the use of the mean atomic number (MAN) background correction [43], which consists of calibrating an absorption-corrected background intensity curve as a function of the average atomic number. This calibration is done by measuring the element of interest in several reference materials, which do not contain this element or a peak interference. Once calibrated, the background is not measured, and the total analysis time is either cut in half, or the extra time is used to double the peak counting time and thus improve the analytical sensitivity especially for HREE in Mnz and LREE in Xnt. This

technique is appropriate for elements above ~200 ppm [44], and thus, is generally applicable to Mnz or Xnt dating (Table 4), as it remains in the range of the detection limit for most REE elements (Fig. 3). To improve accuracy, the shared background method [14] or the use of a "blank correction" [44] using a secondary reference material of known composition is recommended.

5.2.3. Peak interference corrections. The complex composition and the presence of heavy elements in Mnz and Xnt lead to the production of many potential peak interferences. Of major interest for U-Th-Pb_{total} analysis is the correction for interferences of Y-L$\gamma_{2,3}$, Th-Mζ, and La-Lα (n=2) on Pb-Mα, or Ce-Lα (n=2) on Pb-Mβ, and Th-Mγ and K-Kα on U-Mβ (Tables 4, 7). Some interferences are very small, such as the La-Lα (n=2) on Pb-Mα (~0.04 cps/nA on $LaPO_4$; Table 7), yet, they are essential because the Pb-content is low and the La-content in Mnz is high. An extensive discussion on these correction procedures, notably the problem of Y-L$\gamma_{2,3}$ peak shifting between YPO_4 and Mnz, is found in [16]. In order to improve the accuracy of some crucial peak interference corrections such as those applicable to U-Mβ and Pb-Mα, the multipoint background acquisition method is used (see [14]).

The REEs also mutually interfere, which complicates the analysis of REE minerals in general. Fortunately, an improved correction routine that properly corrects for mutual interferences is used in this study [45]. A summary of all possible interferences and the count rates on primary and interference standards is listed in Tables 3 and 6, along with an approximation of the percentage correction for each interference:

$$\%_{interference} \approx \frac{I^A_{interf}/C^B_{interf}}{I^A_{std}/C^A_{std}} * \frac{C^B_{unk}}{C^A_{unk}} \quad (7)$$

where I^A is the measured intensity at the spectrometer position of the measured element A, C^A and C^B are the concentration in weight% of element A and B, and *std*, *interf*, and *unk* stands respectively for the primary standard for element A, the interference standard, and the unknown. This calculation does not consider the matrix effect, which is variable depending on the exact composition of the unknown, yet it is a first-order approximation for the strength of a possible interference. Based on these approximations, interferences can be classified as important, minor (up to ~2 % correction), or too small to be significant (<0.5 % correction; Table 7).

The choice of the optimal X-ray lines depends on whether Mnz or Xnt is being analysed. For example, Pb-Mα is recommended for Mnz as it provides the highest count rate and thus the lowest detection limit. However, it should be avoided and replaced by the measurement of Pb-Mβ in Xnt due to the strong interference from Y-L$\gamma_{2,3}$. Pb-Mβ is only interfered by Ce-Lα (n=2), but this can be ignored in the case of Xnt as the Ce-content is always very low. Two other problematic X-ray lines are Gd-Lβ and Eu-Lβ. These lines are respectively interfered by Ho-Lα and Dy-Lα, which are minor elements in Mnz, and minor to major in Xnt. For Xnt analysis,

Table 7. Summary of peak interference corrections, count rates, and estimate of interference correction. Measurement done on J-type (TAP) or L-type (PET-L, LiF-L) spectrometers on a JEOL-8230.

Measured element				Monazite*		Xenotime*		Interfering element			Approx. % interf. corr.			
Element	Xtal	Standard	cps/nA	Avg wt%	Max wt%	Avg wt%	Max wt%	Interference	Interf. Std.	cps/nA	Mnz avg	Mnz max	Xnt avg	Xnt max
Y Lα	TAP	YPO_4	336.6	0.85	4.92	35.44	41.89	Sr $L\beta_x$	$SrCO_3$	4.60	**0.2%**	**9.2%**	*No data for Sr in Xnt*	
Sr Lα	TAP	$SrSO_4$	362.9	0.10	7.04	?	?	Si Kβ + sat.	Orthoclase	2.98	**0.8%**	**6.0%**		
Si Kα	TAP	Orthoclase	581.0	0.43	3.08	0.15	0.61	Nd Lα (III)	$NdPO_4$	0.62	**1.2%**	**3.3%**	*<0.1%*	*0.3%*
As Lα	TAP	As-pyrite	201.3	0.10	25.56	0.15	0.15	Tb Mβ	$TbPO_4$	7.85	*<0.1%*	*0.4%*	**4.9%**	**8.4%**
								Dy Mα	$DyPO_4$	5.67	0.3%	2.1%	**27.5%**	**39.7%**
								Sm Mγ	$SmPO_4$	1.70	0.4%	2.1%	0.8%	2.9%
Th Mα	PET	ThO_2	114.2	5.56	30.71	0.34	7.42	*No significant interference*						
Ca Kα	PET	F-apatite	684.9	0.80	14.94	0.03	0.17	*No significant interference*						
S Kα	PET	As-pyrite	52.3	0.29	1.36	0.02	0.04	*No significant interference*						
U Mβ	PET	UO_2	252.0	0.60	13.79	0.56	5.13	K Kα	Orthoclase	7.40	*Variable (fluorescence)*			
								Th Mγ	ThO_2	2.10	**7.7%**	**42.5%**	**0.5%**	**11.1%**
								Sm $L\beta_{2,15}$ (II)	$SmPO_4$	0.17	0.3%	1.2%	*0.1%*	*0.3%*
K Kβ	PET	Orthoclase	18.5	Nominally 0 wt%, intensity depends on secondary fluorescence effect				U Mγ	UO_2	4.10	*Variable (fluorescence)*			
								Tm Lα (II)	$TmPO_4$	6.70	*Variable (fluorescence)*			
								Ca Kα	F-apatite	0.55	*Variable (fluorescence)*			
Pb Mα	PET	Pyromorphite	141.2	0.23	1.46	0.17	0.37	Y $L\gamma_{2,3}$	YPO_4	0.51	**2.1%**	**12.0%**	***Prefer Pb Mβ***	
								Th Mζ	ThO_2	0.22	**3.2%**	**17.8%**	**0.3%**	**6.0%**
								La Lα (II)	$LaPO_4$	0.04	**1.9%**	**3.9%**	*<0.1%*	*<0.1%*
La Lα	LiF	$LaPO_4$	62.2	12.11	24.86	0.07	0.14	Nd Ll	$NdPO_4$	0.18	0.2%	0.6%	0.8%	2.8%
Ce Lα	LiF	$CePO_4$	78.2	24.67	32.83	0.17	0.46	*No significant interference*						
Nd Lα	LiF	$NdPO_4$	98.9	9.43	26.00	0.20	0.69	Ce Lβ	$CePO_4$	0.45	1.2%	1.6%	0.4%	1.1%
								La $L\beta_6$	$LaPO_4$	0.36	0.5%	1.0%	*0.1%*	*0.3%*
Pr Lβ	LiF	$PrPO_4$	59.2	2.85	10.77	0.05	0.09	*No significant interference*						
Sm Lβ	LiF	$SmPO_4$	78.6	1.63	7.60	0.47	1.65	Tb Lα	$TbPO_4$	0.60	*<0.1%*	*0.2%*	1.0%	1.7%
Tb Lα	LiF	$TbPO_4$	144.7	0.12	0.34	0.61	1.06	Sm Lβ	$SmPO_4$	0.56	**1.2%**	**3.3%**	*0.1%*	*0.5%*
Eu Lβ	LiF	$EuPO_4$	82.8	0.35	1.00	0.21	0.73	Dy Lα	$DyPO_4$	17.90	**23.0%**	**141%**	***Prefer Eu Lα***	
Dy Lα	LiF	$DyPO_4$	184.1	0.39	2.36	4.81	6.95	*No significant interference*						
Er Lα	LiF	$ErPO_4$	199.8	0.15	1.12	2.15	5.77	Tb Lβ	$TbPO_4$	12.30	**5.2%**	**14.6%**	**1.8%**	**3.1%**
Gd Lβ	LiF	$GdPO_4$	156.4	1.26	3.60	2.89	7.95	Ho Lα	$HoPO_4$	126.50	**6.1%**	**14.8%**	***Prefer Gd Lα***	
								Sm $L\beta_{2,x}$	$SmPO_4$	0.23	0.2%	0.9%	*<0.1%*	*0.1%*
Tm Lα	LiF	$TmPO_4$	207.6	0.14	0.42	1.90	4.55	Sm Lγ	$SmPO_4$	20.30	**116%**	**542%**	**2.5%**	**8.7%**
								Dy Lβ	$DyPO_4$	1.73	**2.3%**	**13.9%**	**2.1%**	**3.0%**
								Gd $L\beta_{9,10}$	$GdPO_4$	0.65	**2.8%**	**8.1%**	0.5%	1.3%
Yb Lα	LiF	$YbPO_4$	209.9	0.08	0.39	1.91	10.01	Tb $L\beta_{2,15}$	$TbPO_4$	0.95	0.7%	2.0%	*0.2%*	*0.3%*
								Dy $L\beta_{3,6}$	$DyPO_4$	0.88	**2.1%**	**13.2%**	1.1%	1.6%
								Sm $L\gamma_2$	$SmPO_4$	0.50	**5.3%**	**24.7%**	*<0.1%*	*0.2%*
Ho Lβ	LiF	$HoPO_4$	114.0	0.10	0.24	1.90	7.10	Yb Lα,n	$YbPO_4$	0.41	0.3%	1.4%	0.4%	1.9%
								Dy $L\beta_{2,15}$	$DyPO_4$	0.24	0.3%	2.5%	0.2%	0.6%
P Kα	PET	$CePO_4$	95.4	12.42	14.23	14.98	16.47	Y Lβ	YAG	0.26	*<0.1%*	*<0.1%*	*0.2%*	*0.2%*

For xenotime only

Pb Mβ	PET	Pyromorphite	*Not determined*	Ce Lα (II)	*Not determined (insignificant in Xnt)*
Eu Lβ	LiF	EuPO4	*Not determined*	Pr $L\beta_{2,15}$, Ce $L\gamma_5$, La Lγ	*Not determined (insignificant in Xnt)*
Gd Lβ	LiF	GdPO4	*Not determined*	Nd $L\beta_{2,15}$, La $L\gamma_{2,3}$	*Not determined (insignificant in Xnt)*

Bold: important correction. Normal: minor correction. *Italic red: very minor correction less than 0.5 % that can be ignored.*

* Various Mnz and Xnt compositions obtained by the authors and from various sources in the literature.

Gd-Lα and Eu-Lα are preferred as they are only interfered by elements present in trace amounts in Xnt (Nd-$L\beta_{2,15}$ and La-$L\gamma_{2,3}$, and by Pr-$L\beta_{2,15}$, Ce-$L\gamma_5$ and La-Lγ, respectively). In any case, accurate results can be obtained providing that all major interferences are properly corrected.

5.3.4. Beam damage. The use of a focussed beam with high current and long counting time in REE-phosphate likely leads to beam damage effects and inaccurate results. In the case of Mnz or Xnt, beam damage leads to the loss of P within the first couple minutes of analysis, and the apparent gain of other elements, especially REE and Th, and even Pb-Mα (Fig. 5a). The effect is strong with a 20 nm C-coating, and can be lowered by using a dual (Al+C)-coating (Fig. 5b). Beam damage appears to be less important in Xnt, most likely due to its slightly higher thermal conductivity compared to Mnz [46, 47]. Better coating such as Au or Ag can help further, yet they are not recommended as they produce additional X-ray lines and absorption edges that complicates the analysis near Pb-Mα (Au) and near U-Mβ and T- Mα (Ag). Also, these heavy metals have much higher absorbance compared to Al or C.

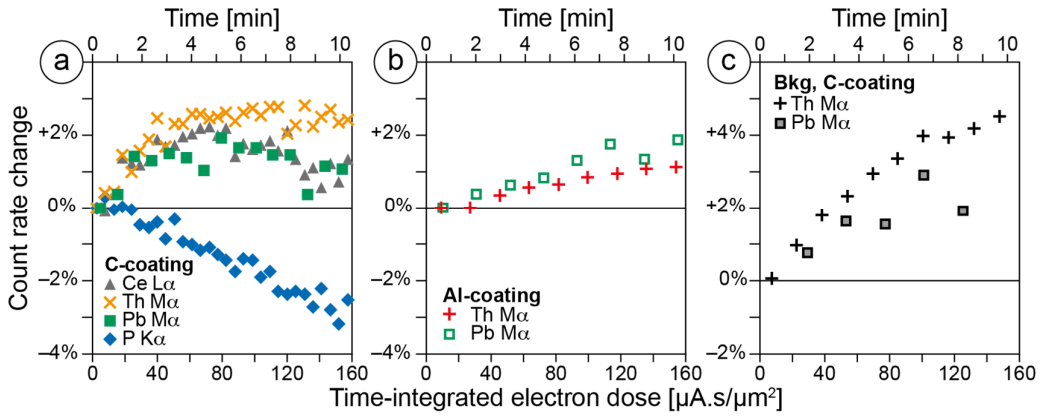

Figure 5. Count rate variation in Burnet Mnz as function of the time-integrated accumulated electron dose a) for Ce-Lα, Th-Mα, Pb-Mα, and P-Kα with 20 nm C-coating, b) for Th-Mα and Pb-Mα with a dual (Al+C)-coating, and c) on background for Th-Mα and Pb-Mα with C-coating. Analytical conditions: 15 keV, 200 nA, focussed beam.

Beam damage can be corrected on the first element analysed on each spectrometer using a time dependent intensity (TDI) or sub-counting correction by dividing the total counting time into several time intervals, and regressing these data to determine the intensity at time t = 0 s. For all other elements, it is desirable to minimize the beam damage effect, which can be done by ensuring their analysis is over before the beam damage is too strong. Two alternative solutions are either to analyse the major elements separately (e.g., at low current) and then only the trace elements at higher current, or to use the EDS to analyse P-Kα and the major REE (e.g., Ce, La, Nd, Pr, and Sm in Mnz). In this paper, a time dependent intensity correction is applied on U-Mβ, Th-Mα, and Pb-Mα, and P-Kα is analysed by EDS, as this line is mostly free of any major interference. Work is in progress to evaluate the feasibility of major REE analysis by EDS (see below).

Another undesirable effect of beam damage is the increase in background intensity over time (e.g., Fig. 5c with C-coating). Although this effect is mostly undetectable when measuring a

major or a minor element, it becomes important when measuring trace amounts. It is assumed that the densification of the matrix, an increase in space charge, and a change in the coating properties (degradation, contamination) ultimately result in a general loss of P and apparent gain in Th and REE, which is visible as a white spot surrounded by a dark rim in BSE after the analysis. This effect is clearly observed when running a blank test (see details in [14]), where the blank test results on Pb-Mα are significantly negative around -50 to -100 ppm when the background is only measured after the 10 min of counting on the peak. To counteract this effect, it is necessary to obtain a "fresh" background measurement, which is done by measuring only the background on the first point, and only the peak on the next analysis points measured right after the background analysis; the background measurement obtained on the first point is then applied on the next peak-only measurement points.

6. APPLICATIONS

A study of an Archean aluminous quartzite from South-West Montana [48] is considered to illustrate the use of the monazite U-Th-Pb_{total} analysis in a simple case with significant Pb-content. The samples are sillimanite+garnet bearing quartzite taken a few kilometres apart. Three samples were selected for a full thin section map in order to identify all monazite. In each sample, 5 to 20 monazite grains (depending on availability) were mapped using the quantitative analysis method described above. Additional examples from the Upper Granite Gorge of the Grand Canyon [49] and from low-Pb monazite dating in low grade metasediments from upstate New York [15] are also considered.

6.1. Results

After petrological examination, samples were coated with 20 nm Al-coating and a 7 - 10 nm overlay of C-coating. The WDS full thin section element maps revealed all accessory phases, especially Mnz (e.g., Fig. 6a). Seven Mnz grains were identified in sample AA09-34B, five of which were then mapped to highlight compositional variation of the key elements Y, Si, Ca, Th and U (Figs. 6b to 6f). These element maps were quantified with standards using the programme "CalcImage" from Probe Software, Inc. For accurate quantification, all elements should be measured, but this task is unrealistic, as it would require obtaining maps for all other major and minor elements, notably REEs and P, or to know the Mnz composition of each homogeneous domain. Instead, the composition of the missing elements can be constrained with some assumptions. With the exception of Si-rich Mnz, the phosphorous content can be assumed to be constant around 28 - 32 and 34 - 38 wt% P_2O_5 for Mnz and Xnt, respectively, and the remaining non-analysed elements are chiefly REEs. In order to test the accuracy of such a quantitative mapping, five distinct fixed compositions were tested: a) no specified element (only the analysed elements are considered in the calculation), b) a Gd-rich, or c) a Ce-rich Mnz (30 wt% P_2O_5; Gd_2O_3 or Ce_2O_3 by difference), d) a Ce-rich Mnz with a lower P_2O_5 content (25 wt%), or e) an average monazite composition (30 wt% P_2O_5; 13 wt% La_2O_3; 3 wt% Pr_2O_3; 11 wt% Nd_2O_3;

2.5 wt% Sm_2O_3; 2 wt% Gd_2O_3; Ce_2O_3 by difference). All maps were corrected using the MAN background correction. Results obtained in a strongly zoned monazite were identical within the error, except when the non-analysed elements were not constrained (Figs. 6g and 6h).

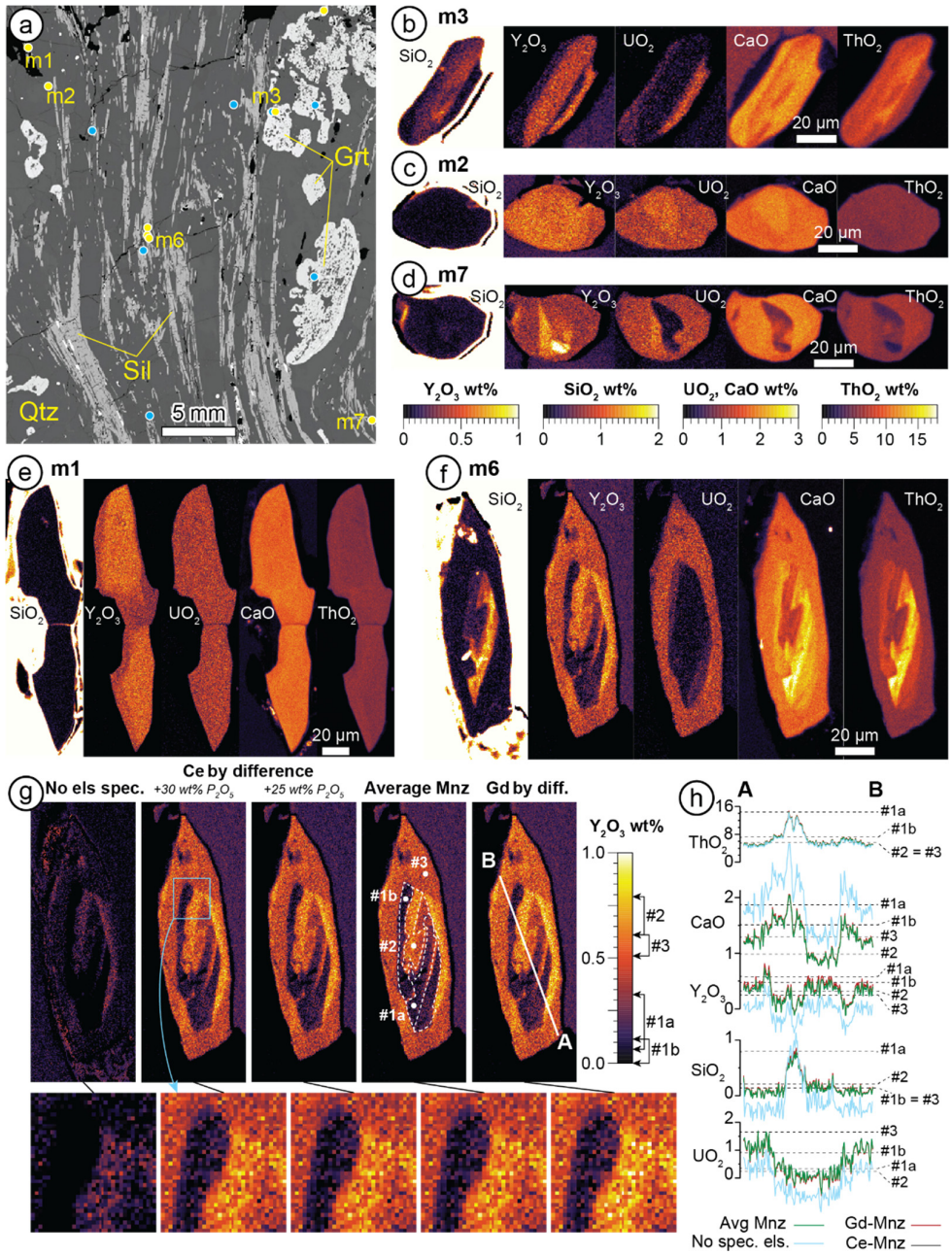

Figure 6. a) BSE image from a full thin section WDS map in sample AA09-34B with the identification of Mnz grains (yellow dots) and zircon (blue circles). b-f) Quantitative element maps of SiO_2, Y_2O_3, UO_2, CaO and ThO_2 in the Mnz identified in a). g) Comparison of quantitative element maps of Y_2O_3 assuming different specified composition for the non-analysed elements (see text for detail). The variation of composition in each domain is highlighted by arrows on the colour scale. h) Cross-section A-B for the calculated composition at the various fixed compositions (analyses of points #1a and #3 in Table 8).

Table 8. Results of quantitative analysis in sample AA09-34B and the Moacyr and Burnet age reference standards. Age in Ma (million year). Values below detection limit or negative are kept for comparison.

		Burnet	Moacyr	AA09-34B				
		Age ref. standard	*Age ref. standard*	**m6**	**m7**	**m6**	**m7**	**m2**
				Core #1a	**Core**	**Rim #3**	**Rim**	**All grain**
	Age	**1085** *±14*	**505** *±10*	**2421** *±20*	**2478** *±90*	**1717** *±4*	**1730** *±14*	**1757** *±26*
P_2O_5	EDS	27.45	28.35	28.22	30.18	30.01	29.56	29.83
SiO_2	MAN	1.38	1.07	1.28	0.11	0.18	0.36	0.09
CaO	MAN	0.85	0.46	2.43	0.86	1.74	1.89	1.84
Y_2O_3	MAN	0.50	1.22	0.11	0.94	0.38	0.26	0.45
La_2O_3	Shared	9.27	14.56	13.61	16.67	15.54	15.58	15.49
La_2O_3	**MAN**	**9.26**	**14.54**	**13.57**	**16.64**	**15.51**	**15.55**	**15.45**
La_2O_3	*EDS*	*9.6*	*14.9*	*14.0*	*17.3*	*16.1*	*16.0*	*16.0*
Ce_2O_3	Shared	29.38	29.05	23.55	29.46	26.84	26.67	26.65
Ce_2O_3	**MAN**	**29.34**	**29.02**	**23.47**	**29.40**	**26.77**	**26.60**	**26.56**
Ce_2O_3	*EDS*	*29.7*	*29.1*	*24.2*	*29.3*	*27.5*	*26.5*	*26.8*
Pr_2O_3	Shared	3.54	3.23	2.37	2.94	2.67	2.60	2.65
Pr_2O_3	**MAN**	**3.57**	**3.29**	**2.37**	**2.98**	**2.67**	**2.59**	**2.65**
Pr_2O_3	*EDS*	*3.2*	*3.3*	*2.9*	*2.9*	*3.6*	*3.0*	*2.7*
Nd_2O_3	Shared	9.44	11.14	8.19	10.66	9.40	8.99	9.35
Nd_2O_3	**MAN**	**9.44**	**11.14**	**8.16**	**10.65**	**9.37**	**8.96**	**9.33**
Nd_2O_3	*EDS*	*9.8*	*10.6*	*8.2*	*10.8*	*9.6*	*9.2*	*9.7*
Sm_2O_3	Shared	3.30	1.87	1.09	1.84	1.46	1.33	1.56
Sm_2O_3	**MAN**	**3.33**	**1.90**	**1.14**	**1.88**	**1.56**	**1.39**	**1.61**
Sm_2O_3	*EDS*	*3.9*	*2.2*	*0.9*	*2.0*	*0.8*	*1.2*	*1.5*
Eu_2O_3	Shared	*-0.09*	*-0.03*	0.09	0.18	0.24	0.22	0.23
Eu_2O_3	**MAN**	***-0.08***	**0.00**	**0.14**	**0.23**	**0.36**	**0.32**	**0.28**
Gd_2O_3	Shared	1.40	0.85	0.68	1.36	1.06	0.93	1.20
Gd_2O_3	**MAN**	**1.48**	**0.85**	**0.66**	**1.41**	**1.02**	**0.85**	**1.18**
Tb_2O_3	Shared	0.26	0.08	0.02	0.14	0.02	0.03	0.09
Tb_2O_3	**MAN**	**0.26**	**0.10**	**0.04**	**0.16**	**0.08**	**0.07**	**0.11**
Dy_2O_3	Shared	0.94	0.24	0.12	0.44	0.18	0.16	0.24
Dy_2O_3	**MAN**	**0.93**	**0.23**	**0.09**	**0.43**	**0.17**	**0.13**	**0.23**
Ho_2O_3	Shared	0.09	0.03	0.04	0.07	0.01	0.00	0.02
Ho_2O_3	**MAN**	**0.01**	***-0.01***	***-0.07***	**0.00**	***-0.06***	***-0.08***	***-0.04***
Er_2O_3	Shared	0.13	0.05	0.01	0.06	0.03	0.02	0.02
Er_2O_3	**MAN**	**0.09**	**0.03**	***-0.04***	**0.03**	***-0.01***	***-0.03***	***-0.02***
Tm_2O_3	Shared	0.01	0.00	0.01	0.01	0.00	0.00	*-0.01*
Tm_2O_3	**MAN**	**0.00**	**0.01**	***-0.03***	**0.01**	***-0.01***	***-0.02***	***-0.01***
Yb_2O_3	Shared	0.03	0.02	0.01	0.00	*-0.01*	*-0.01*	*-0.01*
Yb_2O_3	**MAN**	**0.01**	**0.01**	***-0.05***	***-0.01***	***-0.03***	***-0.04***	***-0.03***
ThO_2	MPB	9.93	6.59	15.16	2.49	6.15	7.05	5.93
UO_2	MPB	0.29	0.12	0.32	0.86	1.88	1.71	2.07
PbO	MPB	0.51	0.15	1.78	0.66	0.98	1.01	1.04

Quantitative analysis was obtained on compositionally homogeneous domains of the unknown and on the Mnz age consistency standards Moacyr and Burnet to obtain U-Th-Pb_{total} ages (Table 8). L-type spectrometers were used for all elements except Y, Si, Sr and As (Table 4). The measurement of U, Th and Pb was performed using the multipoint background correction for improved accuracy on the background measurement, and up to 8 background positions were measured for 50 s each (Table 6). The TDI correction was applied on U, Th and Pb measurements to correct for the beam damage effect. The background was measured only on

the first analysis point, followed by 4 to 8 points with a peak-only measurement. Three distinct analytical methods were evaluated to measure the REEs (Table 8): a) a shared background, or b) a MAN background correction on WDS measurement, and c) an analysis of LREE on EDS combined with a MAN background corrected WDS analysis of the other REE (combined EDS-WDS analysis). Using the element maps, several representative Mnz domains were targeted in sample AA09-34B. Lead-content in all these domains is relatively high (> 0.5 wt%), as the actinide-content is high and the age is old (≥ 1.7 Ga). Whereas the cores commonly show a high Th-content and low U-content, the rims are typically enriched in U. A mixture of cheralite and huttonite/thorite substitutions explains the substitution of Th and U in these monazite domains, with a clear predominance of the cheralite substitution as suggested by the higher Ca-content compared to Si. Work is still in progress, and several samples from this area remain to be dated. Yet, results obtained in this sample yield two distinct clusters of ages, with the Mnz cores yielding an Archean age around 2.4 Ga, and the rims yielding a Paleoproterozoic age around 1.74 Ga (Table 8; [50]).

6.2. Discussion

Tests on the quantitative element maps (Fig. 6) suggest that an average Mnz composition is sufficient to obtain accurate measurements in these low precision element maps, with minor differences in matrix correction depending on the fixed value attributed to the non-analysed elements. However, it remains necessary to constrain the composition of the non-analysed elements, especially the REEs, for instance with an average monazite composition (e.g., 30 % P_2O_5, some LREE, and Ce_2O_3 by difference). The quantified maps are extremely valuable for one-to-one comparison of the various compositional domains within a single sample, and even between various samples. For instance, the Y-rich cores of Mnz grains m6 and m7 (compare Figs. 6d and 6f) are similar and likely to be representative of the same event, whereas the composition of grains m1, m2 (Figs. 6c and 6e) and the rims of grains m6 and m7 is similar, as confirmed by the quantitative point analysis (Table 8). The analyst can thus select some unique compositional domains to be analysed, rather than randomly measuring domains and grains. Overall, this process increases the chance of measuring all age domains in a sample and increases the efficiency in that the number of repeated analyses of a particular compositional domain can be limited to the number needed for a statistically significant weighted mean.

Results of quantitative analysis of REE by WDS are identical within the error for all major and minor elements, independent of the background correction method. A slightly better accuracy is suggested from the shared background method for elements close to their respective detection limit, notably Yb and Ho, as suggested by the minor amount of analysis with slightly negative results compared to the results of the MAN background correction (Table 8). It should be emphasized that the MAN background correction method is suitable mostly for elements above 200 - 500 ppm, and if a better accuracy is required, the use of the shared background [14] or the MAN background correction with a blank correction [44] is recommended. The “blank” correction can be done using a standard with a precisely known trace amount of the element to be corrected, providing that this standard has a composition close to the analysed material.

Results for the major and some minor REEs by EDS are satisfactory, although the calculated compositions have a lower precision. To further evaluate this, analysis of several Mnz reference materials was done on a JEOL JSM-6390 SEM equipped with a 30 mm^2 Thermo UltraDry SDD EDS detector (Table 9) using the standard intensities (same standard as for WDS analysis) and the recommended software defaults for peak shape [51]. A one-minute analysis at 25 % deadtime (beam current ~ 2.5 nA) on this instrument yielded a counting statistics error of 4 - 7 % error for elements above 10 wt%, 10 - 15 % error at 5 - 10 wt%, and 15 - 25 % error at up to 2 wt%. Results are within the error identical with the WDS analysis. EDS analysis might thus be recommended for low precision analysis of major REE (e.g., La, Ce, Pr, Nd, Sm), and WDS should be preferred for REE below 2 wt% or for any REE for which a higher precision is desired. Unfortunately, it is currently impossible to ascertain the accuracy of the EDS versus the WDS analysis due to the lack of independent measurements. Although work is still in progress for the combined analysis of EDS and WDS, it appears feasible to measure several major REE elements, along with phosphorous by EDS, which would ultimately offer a longer analysis time on WDS to measure the minor and trace REE.

Table 9. EDS analysis of several Mnz reference materials (60 s counting).

	Burnet			Moacyr			Bananeira			Diamantina			RT-87		PR-88 hi-Th		PR-88 low-Th		
	WDS	EDS	EDS	**WDS**	EDS	EDS	**WDS**	EDS	EDS	**WDS**	EDS	EDS	**WDS**	EDS	**WDS**	EDS	**WDS**	EDS	EDS
Age	**1115**	-	-	**508**	-	-	**518**	-	-	**694**	-	-	**445**	-	**327**	-	**323**	-	-
P_2O_5	**28.18**	27.1	27.0	**28.38**	27.8	27.4	**29.17**	28.9	29.0	**30.39**	29.8	29.6	**29.41**	28.3	**27.97**	28.3	**28.96**	29.4	28.2
Y_2O_3	**0.90**	0.8	1.0	**1.43**	1.2	1.9	**1.53**	1.4	1.7	**1.08**	0.9	1.4	**2.50**	3.9	**2.48**	2.7	**3.62**	2.9	5.2
CaO	**1.36**	1.2	1.2	**0.53**	0.5	0.5	**1.03**	0.9	0.9	**0.15**	0.1	0.2	**1.28**	1.6	**1.15**	1.1	**1.12**	0.9	1.0
SiO_2	**0.98**	1.7	1.4	**1.18**	1.3	1.1	**0.60**	0.6	0.2	**0.42**	0.0	0.0	**0.21**	0.4	**0.53**	0.9	**0.25**	0.6	0.6
La_2O_3	**8.45**	8.4	8.3	**14.65**	14.1	14.5	**11.08**	10.9	11.2	**15.29**	15.2	15.3	**12.99**	12.9	**11.51**	11.4	**11.41**	12.0	11.8
Ce_2O_3	**27.96**	27.1	27.5	**30.20**	28.8	29.2	**27.10**	26.3	27.2	**32.71**	32.0	32.1	**28.32**	27.4	**25.62**	24.7	**25.66**	25.9	25.6
Nd_2O_3	**9.34**	9.0	7.7	**11.69**	11.0	9.7	**11.79**	11.0	10.1	**12.82**	12.2	10.4	**12.02**	9.9	**10.93**	10.6	**11.21**	10.8	10.0
Pr_2O_3	**3.45**	3.4	3.6	**3.27**	3.2	3.3	**3.39**	3.2	3.7	**3.43**	3.7	3.3	**3.18**	3.0	**2.91**	2.9	**2.96**	2.8	3.3
Sm_2O_3	**4.03**	3.9	4.0	**1.95**	1.8	1.7	**5.11**	4.9	4.5	**2.48**	2.0	2.3	**2.01**	1.7	**2.72**	2.7	**2.97**	2.9	2.6
Gd_2O_3	**2.10**	1.6	2.2	**0.95**	0.7	0.7	**3.02**	2.4	3.2	**2.06**	1.4	2.0	**1.51**	1.4	**2.05**	1.6	**2.45**	1.9	2.5
Dy_2O_3	**1.50**	0.6	1.7	**0.31**	0.1	0.3	**0.72**	0.3	0.8	**0.69**	0.3	0.9	**0.79**	0.9	**0.93**	0.4	**1.23**	0.4	1.4
ThO_2	**11.50**	12.2	12.0	**6.94**	7.3	7.2	**6.10**	6.3	6.1	**0.19**	0.2	0.2	**5.03**	5.3	**8.25**	8.4	**5.40**	5.3	5.9
UO_2	**0.35**	0.4	0.1	**0.21**	0.2	0.0	**0.43**	0.4	0.2	**0.06**	0.0	0.0	**0.31**	0.1	**1.38**	1.5	**1.54**	1.3	1.3
PbO	**0.61**	0.4	0.5	**0.16**	0.2	0.2	**0.17**	0.1	0.1	**0.01**	0.1	0.0	**0.11**	0.1	**0.18**	0.2	**0.14**	0.1	0.1
Total	**100.71**	97.9	98.3	**101.86**	98.3	97.7	**101.23**	97.8	99.0	**101.76**	97.9	97.6	**99.67**	97.0	**98.59**	97.4	**98.92**	97.0	99.6

6.3. Interpretation

Once a date has been accurately calculated, it should be put into a context in order to obtain an age of some specific event (i.e., "petrochronology" when linked to a petrological or a tectonic aspect; [37]). The geological context is first considered in order to compare the calculated dates with other ages obtained in the surrounding areas with different methods and minerals. For instance, based on previous works in the Northern Madison Range [48], the set of dates obtained in sample AA09-34B can be interpreted as a maximum deposition age for the quartzite defined by the youngest Archean monazite (~2.42 Ga) and a major metamorphic event affecting the entire area known as the Big Sky orogeny. The latter is dated at 1.77 to 1.72 Ga [48], and is

responsible for the observed granulite facies metamorphism. Results further suggest that the Northern Madison Range in Montana represents a continuous section of the Big Sky orogenic crust [50].

The full thin section map and the individual monazite grains can help to link textural features with the growth of Mnz, for instance by looking at the preferential growth of Mnz in a pressure shadow in a strongly deformed rock [12, 52]. It is also interesting to compare the compositional variation of Mnz grains included in a phase (e.g., garnet) versus those present in the matrix (e.g., sample from the Grand Canyon; Figs. 7a and 7b). Dates obtained in Mnz included in a mineral (e.g., 1.71 Ga for Mnz in garnet; Fig. 7a) can only pre-date the host mineral formation and must be viewed as an inherited age or possibly a prograde metamorphic event. The latter is preferred in this case, as the deposition age of the metasediment is older (≥ 1.74 Ga). By similarity of composition and age, some core domains in Mnz from the matrix can also be linked to this prograde event (e.g., core of m1; Fig. 7a). To further help with the geo-compositional comparison, Mnz or Xnt compositions are commonly normalised to the chondrite composition, which reflects the average composition of the Earth. Unfortunately, this normalisation usually leads to relatively similar Mnz (or Xnt) profiles due to large difference between chondrite composition (ppm range) and Mnz or Xnt (wt% range). A more sensitive way to compare the data is to normalise the Mnz or Xnt composition to a "reference" Mnz (or Xnt) composition, either taken from the sample itself or from one of the age consistency standards (e.g., compared to Moacyr, Fig. 7b). This normalisation will help to identify subtle enrichment or depletion in a specific REE (see also Fig. 5 in [15]). Other geo-compositional features can also be key in the age interpretation. For instance, it is well recognized that if a Mnz domain grows during the resorption of garnet, an aluminous silicate that preferentially incorporates HREE over LREE, the Mnz will show a higher content in HREE, or it can trigger the growth of Xnt (if thermodynamically stable; e.g. Fig. 7d). In several samples from the Grand Canyon, some Mnz rims and most Xnt yield a significantly younger date around 1.64 Ga (Fig. 7c). This consistency between samples and the fact that Xnt growth is associated with the resorption of garnet (Fig. 7d) strongly suggest that these ages are linked to a late re-equilibration event after the peak of metamorphism, which is dated by the majority of other Mnz around 1.70 - 1.68 Ga. Finally, a few Mnz overgrowths of distinct composition yielded an ill-defined date around 1.4 - 1.5 Ga, which could be interpreted as either an overgrowth or a (partial?) resetting of the age during a dissolution-reprecipitation event involving fluids. Ages obtained in multiple samples from a specific area are then compared, which helps to reinforce the interpretation of specific events, such as those depicted in Fig. 7c [49]. For instance, dating multiple samples was necessary in a study of low-grade Mnz from the Potsdam sandstone (see detail in [15]). In this study, actinide-poor Mnz and Xnt domains with very low Pb-content (≤ 400 ppm) yielded a range of imprecise dates between ca. 500 and 200 Ma, and their interpretation in a single sample was impossible. However, when multiple samples were considered, a pattern of dates emerged and ultimately permitted the dates to be interpreted to represent fluid-events that correlate with the main orogenic events affecting the northern Appalachians between 480 and 250 Ma (see Fig. 8 in [15]).

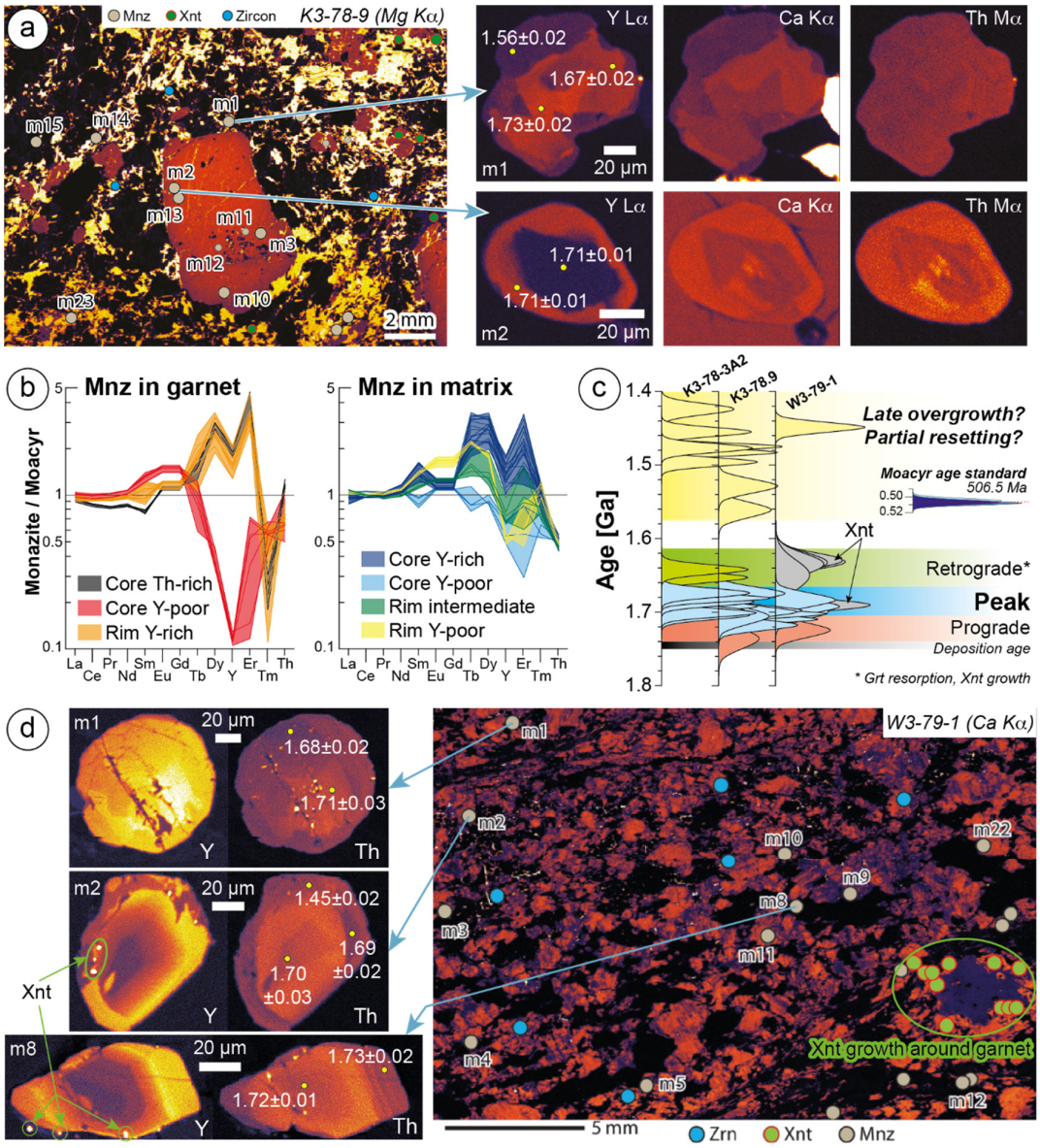

Figure 7. Example of full thin section and Mnz element maps in samples from the Upper Granite Gorge in the Grand Canyon. a) Sample K3-78-9 highlighting the difference in growth zonation of Mnz included in garnet versus Mnz in the matrix. b) Mnz composition (REE+Th) normalised to the Mnz age reference standard "Moacyr". c) Age results in three samples from the Grand Canyon revealing four distinct age groups: inherited, peak of metamorphism, late re-equilibration, and late thermal event. d) Sample W3-79-1 showing the late growth of Xnt associated to the resorption of garnet. Xnt analyses yield ages around 1.65 Ga and is interpreted as a late re-equilibration stage during retrogression.

7. CONCLUSION

The dating of Mnz or Xnt by electron microprobe is a very powerful technique. The microprobe can provide U-Th-Pb_{total} dates at the micron-scale, along with element maps and a complete geo--compositional characterisation of the major and minor elements that compose the Mnz or Xnt. The main limitation of the technique arises from the detectability of trace elements, especially Pb, yet, samples as young as 200 Ma can still be accurately dated with reasonable precision (± 10 - 20 %; see Fig. 2 in [15]). The combination of full thin section compositional mapping to reveal the location of all accessory phases, of high-(spatial)-resolution element mapping of Mnz or Xnt, and of the complete geo-compositional characterization of REE-phosphate strengthens the interpretation of the geological significance of calculated dates. If a sample cannot be dated by EMP due to the low Pb-content, element mapping and geo-compositional analysis of Mnz or Xnt by EMP is critical for establishing an essential understanding of phase compositions and for characterising the compositional zoning and potential polygenetic nature of a grain prior to laser or ion beam analysis. The "age" of a mineral is nearly meaningless if not interpreted in the context of the geological, structural, and/or reaction history.

8. ACKNOWLEDGEMENTS

JMA acknowledges funding from NSF EAR-1427626 and the University of Colorado Boulder for the purchase of the JEOL JXA-8230 microprobe. The authors thank K.H. Mahan for providing information and the authorisation to publish early data in samples from South-West Montana. Additional age reference materials (Diamantina, Bananeira Mnz) and REE-phosphate standards were gratefully provided by G.d.O. Gonçalves and D. Harlov, respectively.

9. REFERENCES

[1] Schoene B 2013 *U-Th-Pb Geochronology* **4**
[2] Parrish R R 1990 *Can. J. Earth Sci.* **27** 1431-1450
[3] Bowles J F W 1990 *Chem. Geol.* **83** 47-53
[4] Parslow G R, Brandstätter F, Kurat G and Thomas D J 1985 *Can. Mineralogist* **23** 543-551
[5] Montel J-M, Veschambre M and Nicollet C 1994 *Compt. Rendus Acad. Sci. Série II* 1489-1495
[6] Montel J-M, Foret S, Veschambre M, Nicollet C and Provost A 1996 *Chem. Geol.* **131** 37-53
[7] Suzuki K, Adachi M and Tanaka T 1991 *Sediment. Geol.* **75** 141-147
[8] Montel J M, Kato T, Enami M, Cocherie A, Finger F, Williams M and Jercinovic M 2018 *Chem. Geol.* **484** 4-15

[9] Suzuki K and Adachi M 1991 *Geochem. J.* **25** 357-376
[10] Suzuki K and Kato T 2008 *Gondwana Res.* **14** 569-586
[11] Shazia J R, Harlov D E, Suzuki K, Kim S W, Girish-Kumar M, Hayasaka Y, Ishwar-Kumar C, Windley B F and Sajeev K 2015 *Lithos* **236-237** 1-15
[12] Williams M L and Jercinovic M J 2002 *J. Struct. Geol.* **24** 1013-1028
[13] Dahl P S, Terry M P, Jercinovic M J, Williams M L, Hamilton M A, Foland K A, Clement S M and Friberg L V M 2005 *Amer. Mineralogist* **90** 1712-1728
[14] Allaz J M, Williams M L, Jercinovic M J, Goemann K and Donovan J 2019 *Microsc. Microanal.* **26** 1-17
[15] Allaz J, Selleck B, Williams M L and Jercinovic M J 2013 *Amer. Mineralogist* **98** 1106-1119
[16] Jercinovic M J and Williams M L 2005 *Amer. Mineralogist* **90** 526-546
[17] Cocherie A, Legendre O, Peucat J J and Kouamelan A N 1998 *Geochim. Cosmochim. Acta* **62** 2475-2497
[18] Scherrer N C, Engi M, Gnos E, Jakob V and Liechti A 2000 *Schweiz. Miner. Petrogr. Mitt.* **80** 93-105
[19] Konečný P, Kusiak M A and Dunkley D J 2018 *Chem. Geol.* **484** 22-35
[20] Overstreet W C 1967 *U.S. Geol. Surv. Prof. Pap.* **530** 327 pp.
[21] Gramaccioli C M and Segalstad T V 1978 *Amer. Mineralogist* **63** 757-761
[22] Bowles J F W, Jobbins E A and Young B R 1980 *Mineral. Mag.* **43** 885-888
[23] Watt G R 1995 *Mineral. Mag.* **59** 735-743
[24] Van Emden B, Thornber M R, Graham J and Lincoln F J 1997 *Can. Mineralogist* **35** 95-104
[25] Seydoux-Guillaume A-M, Wirth R, Heinrich W and Montel J-M 2002 *Eur. J. Mineral.* **14** 869-878
[26] Bulakh A G, R. N A, Zaitsev A N, Pilipiuk A N, Wall F and Kirillov A S 2000 *Neues Jahrb. für Mineral. - Abhandlungen* **5** 217-233
[27] Krenn E, Putz H, Finger F and Paar W H 2011 *Mineral. Petrol.* **102** 51-62
[28] Chen W, Honghui H, Bai T and Jiang S 2017 *Resources* **6** 51
[29] Graeser S and Schwander H 1987 *Schweizerische Mineral. und Petrogr. Mitteilungen* **67** 103-113
[30] Ondrejka M, Uher P, Pršek J and Ozdín D 2007 *Lithos* **95** 116-129
[31] Jercinovic M J, Williams M L and Berman R G 2013 in: *AGU Fall Meet.* V53B–2794
[32] Steiger R H and Jäger E 1977 *Earth Planet. Sci. Lett.* **36** 359-362
[33] Suzuki K and Adachi M 1991 *J. Earth Sci. Nagoya Univ.* **38** 11-38
[34] Jercinovic M J, Williams M L, Allaz J and Donovan J J 2012 *IOP Conf. Ser. Mater. Sci. Engng.* **32** 1-22
[35] Fialin M, Rémy H, Richard C and Wagner C 1999 *Amer. Mineralogist* **84** 70-77
[36] Dumond G, McLean N, Williams M L, Jercinovic M J and Bowring S 2008 *Chem. Geol.* **254** 175-196

[37] Williams M L, Jercinovic M J, Mahan K H and Dumond G 2018 *Electron Microprobe Petrochronology* **83**
[38] Williams M L, Jercinovic M J, Goncalves P and Mahan K H 2006 *Chem. Geol.* **225** 1-15
[39] Goncalves P, Williams M L and Jercinovic M J 2005 *Amer. Mineralogist* **90** 578-585
[40] Gonçalves G O, Lana C, Scholz R, Buick I S, Gerdes A, Kamo S L, Corfu F, Marinho M M, Chaves A O, Valeriano C and Nalini H A 2016 *Chem. Geol.* **424** 30-50
[41] Jercinovic M J, Williams M L and Lane E D 2008 *Chem. Geol.* **254** 197-215
[42] Williams M L, Jercinovic M J and Terry M P 1999 *Geology* **27** 1023-1026
[43] Donovan J J and Tingle T N 1996 *J. Microsc. Microanal.* **2** 1-7
[44] Donovan J J, Singer J W and Armstrong J T 2016 *Amer. Mineralogist* **101** 1839-1853
[45] Donovan J J, Snyder D A and Rivers M L 1993 *Microbeam Anal.* **2** 23-28
[46] Du A, Wan C, Qu Z and Pan W 2009 *J. Amer. Ceram. Soc.* **92** 2687-2692
[47] Hikichi Y, Ota T, Daimon K and Hattori T 1998 *J. Amer. Ceram. Soc.* 81 2216-2218
[48] Kellogg K S and Mogk D W 2009 *Rocky Mt. Geol.* **44** 85-102
[49] Allaz J M, Williams M L and Jercinovic M J 2010 in: *AGU Fall Meet.* V41D-2305
[50] Flynn C, Mahan K H and Allaz J M 2018 in: *AGU Fall Meeting* T42A-08
[51] Seddio S M 2018 in: *M&M 2018 Pre-meeting Congr.* X.61 10-1
[52] Williams M L and Jercinovic M J 2012 *J. Metamorph. Geol*. **30** 739-752